Wavelet-based detection of scaling behavior in noisy experimental data

Y. F. Contoyiannis[*] and S. M. Potirakis [†]

Department of Electrical and Electronics Engineering, University of West Attica, GR-12244 Egaleo, Greece

F. K. Diakonos [‡]

Department of Physics, University of Athens, GR-15784 Athens, Greece

The detection of power laws in real data is a demanding task for several reasons. The two most frequently met are that (i) real data possess noise, which affects the power-law tails significantly, and (ii) there is no solid tool for discrimination between a power law, valid in a specific range of scales, and other functional forms like log-normal or stretched exponential distributions. In the present report we demonstrate, employing simulated and real data, that using wavelets it is possible to overcome both of the above-mentioned difficulties and achieve secure detection of a power law and an accurate estimation of the associated exponent.

I. INTRODUCTION

Scaling relationships of the form

$$F(x) = cx^{-p} \quad \text{for} \quad \Delta_{\max} > x > \Delta_{\min}, \qquad (1)$$

characterized as power laws with characteristic exponent p, valid between the $\Delta_{\min}$ and the $\Delta_{\max}$ scales, are widespread in the analysis of signals occurring in measuring processes. They usually apply as a statistical property related to the tail of a distribution ($x \gg \Delta_{\min}$), describing the "weight" of the value x in a measurement of a physical property X. Specific examples offer the power spectrum $S(f)$ of a signal with f the underlying frequency, encountered in the $\frac{1}{f}$ noise phenomenon, the statistical distribution $N(\tau)$ of the waiting times τ between beats in a heartbeat time series, the distribution of avalance sizes s in self-organized criticality, the distribution of laminar lengths in the (spatial and temporal) order parameter fluctuations in critical systems, etc. [1–3]. In experimental signals, where the statistics are strictly limited, it is often the case that the tail of a calculated distribution is affected by random fluctuations, overriding the expected signal. Thus, although theoretically the presence of the power law is expected to hold in the tail of a distribution, in experimental observations it is restricted to the body of the distribution. This leads to enhanced uncertainty in the characterization of a specific distribution as a power law. In addition, in physical systems, due to the finite size, it is often the case that the condition $\Delta_{\max} \gg \Delta_{\min}$, necessary for a clear signature of power-law behavior, becomes a simple inequality ($\Delta_{\max} > \Delta_{\min}$) so that the range of validity of Eq. (1) is shrinks significantly. Thus, there is only a small part of the related distribution which

follows a power law. Since the region where the power law applies is usually not strictly known, this significantly affects the estimate of the exponent p. Furthermore, in this case other functional forms like log-normal or stretched exponential distributions may describe the recorded data equally well, particularly if both factors (noisy tails, finite-size effects) are present [4].

In this work we demonstrate that the difficulties in the detection of a power law in experimental data can be overcome using wavelets. The idea to apply wavelets for the detection of power laws is not new. There is an extensive literature on this subject [5–12]. The common point of view is to use wavelets for analysis of the time series on which the calculation of an emerging distribution, supposed to follow a power law, is based. The priority in such a search is the recognition of self-similar patterns in the considered time series. Within this framework the use of wavelets as a tool to reduce noise effects is also attempted [13–18]. Here we use the wavelets in a later phase, once the targeted distribution is determined. We show that the information for the appearance of a power law is already contained in the lower-scale coefficients, which turn out to be insensitive to a mixture with noise. Furthermore, we demonstrate that one can locate zones in which scaling behavior applies and the calculation of the associated scaling exponent is safely performed, even in the presence of noise, using these low-scale wavelet coefficients.

In fact, our treatment inverses the problem concerning the search for power-law behavior in experimental data. Instead of fitting with a power law and applying suitable tests to the fitting results, here we consider the imprint of power-law behavior on the properties of low-scale wavelet coefficients and we test the appearance of these properties in the statistical distributions obtained from the measured data. There are two significant advantages of the proposed method: (i) robustness against the admixture of noise and (ii) accurate determination

---

[*]yiaconto@uniwa.gr

[†]spoti@uniwa.gr

[‡]fdiakono@phys.uoa.gr

of windows of scales in which the power-law description applies.

In the following, we first extract the wavelet-coefficient properties we use as a benchmark for the power-law appearance. These properties form the theoretical platform for the subsequent analysis. Then we apply the developed criteria to a noise-infected power-law distribution, at various noise amplitudes, demonstrating the robustness of the proposed approach. Next we apply the proposed method to simulated data, in particular, to the distribution of the waiting times in the neighborhood of 0 (stable fixed point of the effective potential) in a three-dimensional (3D) Ising magnetization time series at the corresponding (pseudo)critical temperature. This distribution attains a power-law form as shown in [19]. Finally, we show the practical use of the proposed scheme, applying it to a variety of distributions originating from experimentally determined time series.

II. POWER-LAW-INDUCED CONSTRAINTS TO WAVELET COEFFICIENTS

We start our discussion with the presentation of some properties of the wavelets which are relevant for the following analysis. In general, the translation and scaling properties of the mother wavelet are given by [20]

$$\psi_{s,t}(x) \equiv \psi_s(x-t) = s^{-m}\psi\left(\frac{x-t}{s}\right),$$

with s and t the scaling and the translation parameters, respectively. In discrete form, using the scaling exponent $m = \frac{1}{2}$ and expressing scaling and translation parameters in powers of 2, using $s = 2^{-j}$ and $t = 2^{-j}k$, an arbitrary element of the wavelet basis is written as

$$\psi_{j,k}(x) = 2^{\frac{j}{2}}\psi(2^j x - k), \quad j,k \in \mathbb{Z}, \quad (2)$$

with $j = \ldots, -1, 0, 1, \ldots$ and $k = -j, \ldots, -1, 0, 1, \ldots, j$. Any function $F(x)$ can be expanded in such a wavelet basis as

$$F(x) = \sum_{j=-\infty}^{\infty}\sum_{k=-\infty}^{\infty} d_{j,k}\psi_{j,k}(x), \quad (3)$$

with

$$d_{j,k} = \int_{-\infty}^{\infty} dx\,\psi_{j,k}(x)F(x). \quad (4)$$

In the following we consider a power law of the form, valid for a finite system,

$$F(x) = \begin{cases} 0, & x \notin [\Delta_{\min}, \Delta_{\max}), \\ cx^{-p}, & \Delta_{\max} > x \geqslant \Delta_{\min}, \end{cases} \quad (5)$$

with $p \in \mathbb{R}$ and c a normalization constant since $F(x)$ is assumed to be a distribution. Consequently, $F(x)$ has finite support and the sums in Eq. (3) are restricted to $j \geqslant 0$ and $k \geqslant 0$. For $p < 1$ one can further assume $\Delta_{\min} = 0$ since the function, (5), is integrable around 0 in this case. Then $F(x)$ possesses the scaling property

$$F\left(\frac{x}{b}\right) = b^p F(x), \quad (6)$$

which, combined with Eq. (2) holding for the mother wavelet, leads to

$$d_{j',k'} = \frac{1}{\sqrt{b}}\int_{-\infty}^{\infty} dx\,2^{\frac{j}{2}}\psi\left(2^j\frac{x}{b} - k\right)b^{-p}F\left(\frac{x}{b}\right), \quad (7)$$

with $j' = j - \frac{\ln b}{\ln 2}$ and $k' = k$. Changing variable $x' = \frac{x}{b}$ we find

$$d_{j',k'} = b^{-p+\frac{1}{2}}\int_{-\infty}^{\infty} dx'\,\psi_{j,k}(x')F(x') = b^{-p+\frac{1}{2}}d_{j,k} \quad (8)$$

as the scaling property of the wavelet coefficients when $F(x)$ is of the form of (5) with $p < 1$. Particularly, using $j' = j + 1$, which means $b = \frac{1}{2}$, we find

$$d_{j+1,k} = 2^{p-\frac{1}{2}}d_{j,k}. \quad (9)$$

Defining the ratio $R_{j,k} = \frac{d_{j,k}}{d_{j+1,k}}$ we find

$$R_{j,k} = 2^{\frac{1}{2}-p}, \quad (10)$$

which is independent of j and k. Thus an inherent property of the wavelet decomposition of an ideal power law is that

$$\lambda = \frac{R_{j,k}}{R_{j+1,k}} = 1 \quad \text{for all} \quad j, k. \quad (11)$$

Our proposal is to use this property for the characterization of a power law obtained from a noisy experimentally observed signal. We argue that at coarse scales (small j) the influence of the high-frequency noise is suppressed and relation (11) can filter the power-law behavior. This is clearly demonstrated in the following by calculating λ for several sets of simulated and experimentally measured data. The notion of an "ideal power law" indicated above includes the constraints $p < 1$ and $\Delta_{\min} = 0$. It is still necessary to clarify how relation (11) is modified when $p > 1$ and $\Delta_{\min} > 0$. Note that the condition $p > 1$ necessarily implies that $\Delta_{\min} > 0$ for $F(x)$ in Eqs. (1) and (5), representing a distribution. Additionally, the modification of Eq. (11) when $F(x)$ is replaced by a discrete power-law distribution of the form $F_d(i) \sim i^{-p}$ for $i = i_{\min}, i_{\min} + 1, \ldots, i_{\max}$ should be checked. Such a situation will frequently occur in the examples considered in the following. Then one can bridge the difference in the two descriptions, writing

$$F(x) = c\sum_{i=i_{\min}}^{i_{\max}} \delta(x-i)x^{-p}, \quad (12)$$

and the integral in Eq. (4) leads to the sum

$$d_{j,k} = c\sum_{i=i_{\min}}^{i_{\max}} \psi_{j,k}(i)i^{-p}, \quad (13)$$

where $i_{\min}$ and $i_{\max}$ are determined by the support of $\psi_{j,k}(x)$, i.e., the x interval for which $\psi_{j,k}(x)$ is different from 0. To simplify the notation, in the following, we use uniquely $\Delta_{\min}$ ($\Delta_{\max}$) to denote the minimal (maximal) value of the distributed variable for both discrete and continuous cases. Obviously $\Delta_{\min}$ and $\Delta_{\max}$ will be integers in the discrete case.

III. HAAR ANALYSIS OF POWER-LAW DISTRIBUTIONS

To proceed we continue our study using Haar wavelets [21] for the expansion of a power-law function of the form of Eq. (5), assuming $\Delta_{\min} \geqslant 0$ and $p > 0$. We choose the Haar basis since it is convenient for analytical calculations and it enables the derivation of wavelet coefficient conditions in closed expressions. Nevertheless, all the properties as well as the key property in Eq. (11) presented in the previous section are valid for any choice of the wavelet basis. In the case of the Haar basis the mother wavelet, with nonvanishing values in the interval $(0, \Delta]$, is given as

$$\psi_H(x) = \theta\left(\frac{\Delta}{2} - x\right)\theta(x) - \theta\left(x - \frac{\Delta}{2}\right)\theta(\Delta - x), \quad (14)$$

leading to the Haar wavelet basis,

$$\psi_{j,k}(x) = \theta\left(k\frac{\Delta}{2^j} + \frac{\Delta}{2^{j+1}} - x\right)\theta\left(x - k\frac{\Delta}{2^j}\right)$$
$$- \theta\left(x - k\frac{\Delta}{2^j} - \frac{\Delta}{2^{j+1}}\right)\theta\left((k+1)\frac{\Delta}{2^j} - x\right), \quad (15)$$

with $\theta(z)$ the Heaviside step function [22]. Employing Eq. (4) it is straightforward to calculate the coefficients $d_{j,k}$ for the expansion of $F(x)$, given in Eq. (5), in the Haar basis. We start our calculations for the case $p < 1$ and $\Delta_{\min} = 0$, which is discussed in a more general framework in the previous section. We find

$$d_{j,k} = \frac{c}{1-p}\sqrt{\frac{2^j}{\Delta}}\left[2\left(k\frac{\Delta}{2^j} + \frac{\Delta}{2^{j+1}}\right)^{1-p}\right.$$
$$\left. - \left(k\frac{\Delta}{2^j}\right)^{1-p} - \left((k+1)\frac{\Delta}{2^j}\right)^{1-p}\right]. \quad (16)$$

Clearly, for $p < 1$ and $\Delta_{\min} = 0$ the coefficients $d_{j,k}$ obey the general scaling relations in Eqs. (9)–(11) as expected. As the next step we calculate the coefficients $d_{j,k}$ and the ratios $R_{j,k}$, λ for $p > 1$ and $\Delta_{\min} > 0$. Obviously, for $\Delta_{\min} < k\frac{\Delta}{2^{j+1}}$ the expression in Eq. (16) is still valid and therefore the scaling laws, (9)–(11), are obeyed. In fact, whenever the condition $\Delta_{\min} \ll \Delta$ is satisfied there exists a maximum $j_{\max}$ for which the constraint:

$$\frac{\Delta_{\min}}{\Delta} < \frac{k}{2^{j+1}} \quad (17)$$

is fulfilled. Then, provided that $k \geqslant 1$, Eq. (9) is valid for $j < j_{\max} - 1$, Eq. (10) is valid for $j < j_{\max} - 2$, and Eq. (11) is valid for $j < j_{\max} - 3$. Since $j \geqslant 0$ we find that $j_{\max} \geqslant 3$, which leads to the constraint $\Delta \geqslant 16\Delta_{\min}$, i.e., the scaling law must hold for at least one and a half decades, a reasonable range for physical systems. Note that for the applicability of our approach, we need to consider only the coarse-grained scales (small j), which are less sensitive to the presence of noise, thus the existence of a single set $\{j, j+1, j+2\}$ fulfilling condition (17), i.e., $j = 0$, is sufficient. In this case we have that $\lambda = \frac{d_{0,0}d_{2,0}}{d_{1,0}^2} = 1$ is the relevant condition for the appearance of a power law between the $\Delta_{\min}$ and the Δ scales. Unfortunately, a complication occurs for $k = 0$ since condition (17) is violated. Thus, it requires more effort to handle

this case. Focusing on this, the Haar wavelet coefficients, when $k = 0$ and $\Delta_{\min} > 0$, become

$$d_{j,0} = \frac{c}{1-p}\sqrt{\frac{2^j}{\Delta}}\left[2\left(\frac{\Delta}{2^{j+1}}\right)^{1-p} - \Delta_{\min}^{1-p} - \left(\frac{\Delta}{2^j}\right)^{1-p}\right], \quad (18)$$

leading to

$$R_{j,0} = 2^{\frac{1}{2}-p}\left[\frac{2\left(\frac{\Delta}{2^{j+1}}\right)^{1-p} - \Delta_{\min}^{1-p} - \left(\frac{\Delta}{2^j}\right)^{1-p}}{2\left(\frac{\Delta}{2^{j+1}}\right)^{1-p} - 2\Delta_{\min}^{1-p} - \left(\frac{\Delta}{2^j}\right)^{1-p}}\right]. \quad (19)$$

Equation (19), after some algebraic manipulations, becomes

$$R_{j,0} = 2^{\frac{1}{2}-p}\left[\frac{1 - \frac{1}{2^p-1}\left(\frac{\Delta}{\Delta_{\min}2^j}\right)^{p-1}}{1 - \frac{2}{2^p-1}\left(\frac{\Delta}{\Delta_{\min}2^j}\right)^{p-1}}\right], \quad (20)$$

which now depends on j. However, for $\Delta \gg \Delta_{\min}$ and low values of j the term in brackets is close to $\frac{1}{2}$ and consequently the relation

$$\lambda = \frac{R_{j,0}}{R_{j+1,0}} \approx 1 \quad (21)$$

is still valid.

Particularly for the discrete case, the coefficients $d_{j,k}$ can be written as

$$d_{j,k} = c\sqrt{\frac{2^j}{\Delta}}\left(\sum_{i=\max([k\frac{\Delta}{2^j}],1)}^{[k\frac{\Delta}{2^j} + \frac{\Delta}{2^{j+1}}]} i^{-p} - \sum_{i=[k\frac{\Delta}{2^j} + \frac{\Delta}{2^{j+1}}]+1}^{[(k+1)\frac{\Delta}{2^j}]} i^{-p}\right), \quad (22)$$

where $[z]$ means the integer part of a variable z. Note that although Δ is an integer, the ratio $\frac{\Delta}{2^j}$ is in general not. First, we consider the case $k > 0$. Then, for $\Delta \gg 1$ and low values of j, in which we are interested, $\max([k\frac{\Delta}{2^j}], 1) = [k\frac{\Delta}{2^j}]$ holds and the sum in Eq. (22) can be performed, leading to

$$d_{j,k} = c\sqrt{\frac{2^j}{\Delta}}\left\{\zeta\left[p, \left(k\frac{\Delta}{2^j}\right)\right] + \zeta\left[p, \left((k+1)\frac{\Delta}{2^j}\right)\right]\right.$$
$$\left. - 2\zeta\left[p, \left(k\frac{\Delta}{2^j} + \frac{\Delta}{2^{j+1}}\right) + 1\right]\right\}, \quad (23)$$

where $\zeta(p, s)$ is the Hurwitz zeta function [22]. For $j \leqslant j_{\max}$ with $j_{\max}$ such that $\frac{\Delta}{2^{j_{\max}}} \gg 1$ we can use the asymptotic expansion of $\zeta(p, s)$ for $s \to \infty$,

$$\zeta(p, s) \overset{s\to\infty}{\approx} \frac{1}{2}s^{-p} + \frac{s^{1-p}}{p-1}, \quad (24)$$

to rewrite $d_{j,k}$ as

$$d_{j,k} \approx \frac{c}{p-1}\left(\frac{2^j}{\Delta}\right)^{p-\frac{1}{2}}\left(k^{1-p} - (k+1)^{1-p}\right.$$
$$\left. + \frac{(p-1)2^j}{2\Delta}(k^{-p} - (k+1)^{-p})\right). \quad (25)$$

Since $\frac{2^j}{2\Delta} \ll 1$ Eq. (25) simplifies to

$$d_{j,k} \approx \frac{c}{p-1}\left(\frac{2^j}{\Delta}\right)^{p-\frac{1}{2}}(k^{1-p} - (k+1)^{1-p}), \quad (26)$$

and therefore

$$R_{j,k} \approx 2^{\frac{1}{2}-p} \Rightarrow \lambda \approx 1. \tag{27}$$

When $k = 0$ we find

$$d_{j,0} = c \sqrt{\frac{2^j}{\Delta}} \left\{ \zeta(p, 1) + \zeta \left[p, \left(\frac{\Delta}{2^j} \right) \right] - 2 \zeta \left[p, \left(\frac{\Delta}{2^{j+1}} \right) + 1 \right] \right\}, \tag{28}$$

and employing the asymptotic expansion of $\zeta(p, s)$ for $s \gg 1$ we obtain

$$d_{j,0} \approx c \sqrt{\frac{2^j}{\Delta}} \zeta(p), \tag{29}$$

which in turn leads again to $\lambda \approx 1$. Thus, we have shown that for a power law the quantity λ approaches 1 for $\Delta \to \infty$ in a range of scales which necessarily includes the lowest j values. We show in the following that this property characterizes in a unique manner the presence of power-law behavior in a general data set, constituting the backbone of the search method proposed in the present work. Our strategy is based on the use of the functional dependence of the wavelet coefficients $d_{j,k}$ on Δ (for a power-law distribution) to construct quantities, like λ in Eqs. (11) and (21), which in the limit $\Delta \gg 1$ become independent of Δ. Within this framework, we have to analyze the experimentally recorded signal employing its transforms with Haar wavelets of variable range Δ with $\Delta_{\min} \ll \Delta \leqslant \Delta_{\max}$. Note that in practice $\Delta_{\max}$ is the maximal Δ value for which the considered distribution (often referred to also as the "signal" in the following) is different from 0.

IV. APPLYING THE WAVELET PROTOCOL TO DATA

Based on the analysis in the previous section we present here an algorithm which can be directly applied to experimentally determined distributions, searching for the presence of scaling behavior. To be consistent with the forthcoming applications, we restrict the presentation to the discrete case. The extension to the continuous one is trivial. The proposed algorithm comprises the following steps:

(i) We numerically estimate the ratio λ, based on Eq. (21) for $j = 0, k = 0$, obtained using the formula

$$\lambda = \frac{\frac{d_{00}}{d_{10}}}{\frac{d_{10}}{d_{20}}} = \frac{d_{00} d_{20}}{d_{10}^2}$$

$$= \frac{\left(\sum_{i=1}^{[\frac{\Delta}{2}]} F_d(i) - \sum_{\frac{\Delta}{2}}^{\Delta} F_d(i) \right) \left(\sum_{i=1}^{[\frac{\Delta}{8}]} F_d(i) - \sum_{i=[\frac{\Delta}{8}]}^{[\frac{\Delta}{4}]} F_d(i) \right)}{\left(\sum_{i=1}^{[\frac{\Delta}{4}]} F_d(i) - \sum_{i=[\frac{\Delta}{4}]}^{[\frac{\Delta}{2}]} F_d(i) \right)^2}, \tag{30}$$

where $F_d(i)$, $i = 1, 2, \ldots$, denotes the measured distribution values, and $8 < \Delta < \Delta_{\max}$ ($\Delta_{\max}$ is the length of the signal). According to Eq. (30), we expect that, when the signal possesses a scaling behavior, λ will approach the value $\lambda \approx 1$ for sufficiently large Δ, i.e., $\Delta \gg i_{\min}$. We denote as $I_\lambda(\epsilon_\lambda)$ the interval of Δ values within which λ converges to 1 with a prescribed accuracy ϵ_λ.

(ii) For the interval $I_\lambda(\epsilon_\lambda)$ we calculate the ratio R, defined through the following formula (again using $j = 0, k = 0$):

$$R = \frac{d_{00}}{d_{10}} = \frac{1}{\sqrt{2}} \frac{\left(\sum_{i=1}^{[\frac{\Delta}{2}]} F_d(i) - \sum_{\frac{\Delta}{2}}^{\Delta} F_d(i) \right)}{\left(\sum_{i=1}^{[\frac{\Delta}{4}]} F_d(i) - \sum_{i=[\frac{\Delta}{4}]}^{[\frac{\Delta}{2}]} F_d(i) \right)}. \tag{31}$$

(iii) We locate the interval $I_R \subseteq I_\lambda$ in Δ space, for which the R values stabilize around a mean value $\langle R \rangle$ with accuracy ϵ_R, and we calculate this mean value.

(iv) For estimation of the p exponent we use the discrete version of the test function in Eq. (5), $F_d(i) = ci^{-p}$, $i = 1, 2, 3, 4, \ldots$, and we solve Eq. (31) numerically for the given $\langle R \rangle$ value with respect to p.

At this point some important remarks are in order. First, it is crucial in the analysis to use the $k = 0$ coefficients of the wavelet basis for the lowest values of j. The reason for this is the following: A low j implies a coarse-grained description, which is less sensitive to high-frequency fluctuations of the measured distribution, while higher j values are strongly influenced by these fluctuations. Since the possible k values are bounded by j, when j is low, k is also restricted to low values. The coefficients $d_{j,0}$ for small j describe the bulk of the distribution and therefore are less sensitive to the details of the distribution tail, which is usually affected by statistics and noise. Thus, the choice $k = 0$ reduces the influence of noise and finite statistics on the determination of the quantities λ and R. Second, when the signal is particularly noisy, one may observe dispersed λ values close to 1. In this case, the scaling behavior is only approximate and the noise generates exponential tails which suggest the use of a test function, $\tilde{F}(i) = ci^{-p} e^{-qi}$, $i = 1, 2, 3, 4, \ldots$, in Eq. (31) for the description of the noisy signal. As in the pure power-law case we solve Eq. (31) for the pair (p, q) with the condition $q \ll 1$, which guarantees that the power law, at least approximately, holds, allowing the use of Eq. (31). In practice, the additional parameter q, introduced to estimate the divergence from scaling behavior, leads to a self-consistent description for q values in the interval 0.001–0.01 (empirical result). A more quantitative discussion of these two issues is given in the Appendix.

To demonstrate how this algorithm works in practice, we provide a series of examples, starting from simulated data and extending up to experimentally measured signals. The simulated data are generated as a sequence of uncorrelated random numbers sampled from a specific distribution $P(r)$. Let us denote such a time series by $\{r_n\}$ (with $n = 1, 2, \ldots, N$). We consider three cases: (i) exponentially, (ii) log-normally, and (iii) power-law-distributed r_n. In all cases the length of the corresponding time series is $N = 150\,000$. Noise is added to the considered time series in two ways: (a) multiplicatively, i.e., by transforming r_n to $\tilde{r}_n = r_n(1 + a\xi_n)$ at each step, or (b) additively, with the transform $\hat{r}_n = r_n + a\xi_n$ with ξ_n uniformly distributed in [0,1). We use the term amplitude noise for case (a) and the term additive noise for case (b).

In Fig. 1(a) we show the function $\lambda(\Delta)$ in the noiseless scenario, comparing the result for a power-law distribution with exponent $p = 1.67$ (red circles) to the result corresponding to a slow exponential decay (exponent 0.05; blue stars) and to that for a log-normal distribution with variance $\sigma = 1$
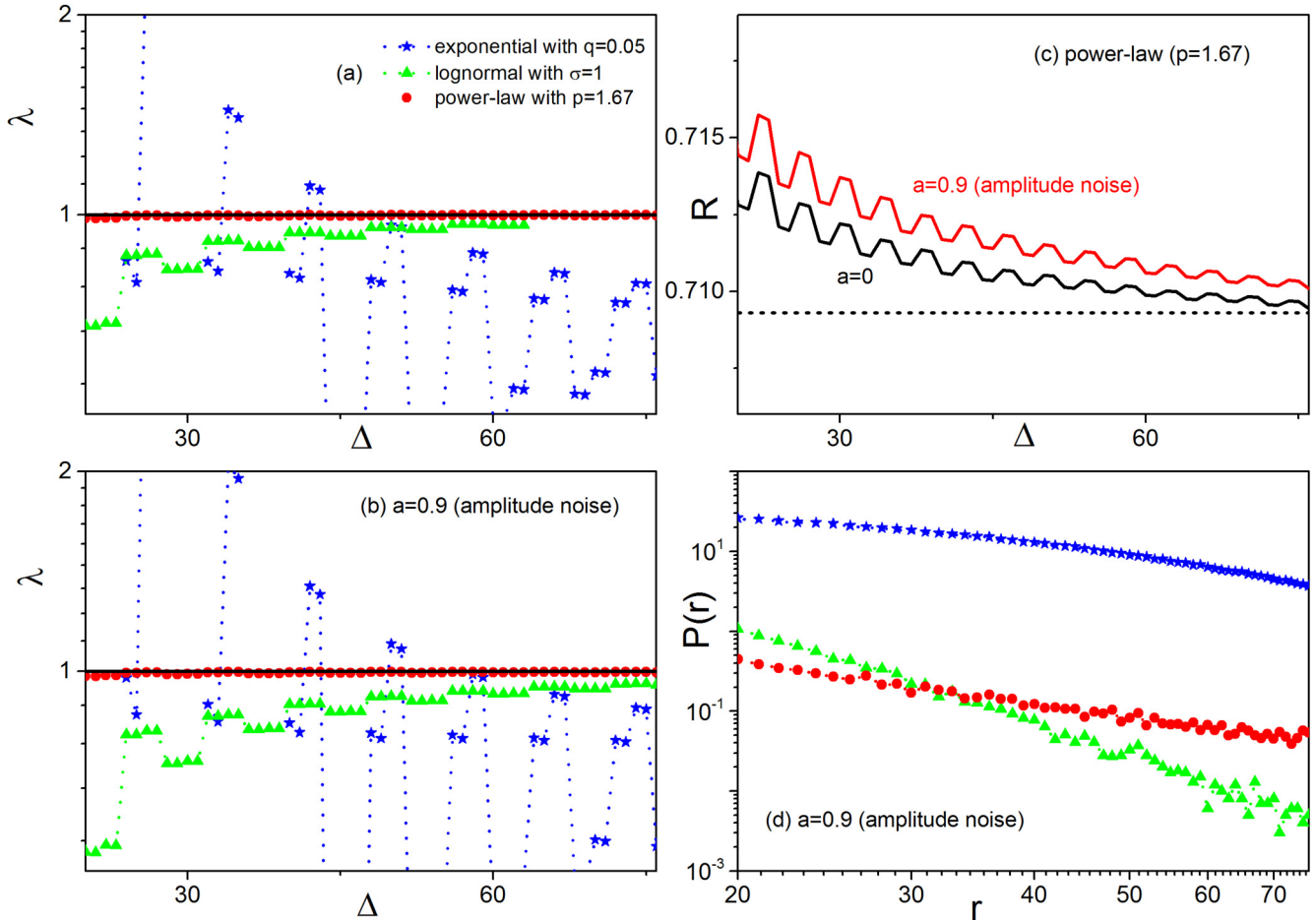
FIG. 1. Synthetic data with amplitude noise. (a) The function $\lambda(\Delta)$ given in Eq. (30), calculated from time series of random numbers distributed exponentially (blue stars), log-normally (green triangles), and as a power law (red circles). The solid black line at $\lambda = 1$ is a guide for the eye. (b) The functions $\lambda(\Delta)$ for similar time series obtained from the time series in (a) adding amplitude noise with $a = 0.9$. (c) The function $R(\Delta)$ for the power-law case in the noiseless (black line) and the noisy (upper, red line) case. Both lines converge to $R \approx 0.71$, leading to $p = 1.68$. (d) Distributions of the time-series values used in (b).

(green triangles). We observe that, for the power law, $\lambda(\Delta)$ converges quite rapidly to 1 and it is clearly distinguished from the other two cases. Note that, since the time series is finite, the distribution $P(r)$ of the r_n values is truncated at Δ_{max}, becoming 0 for larger r values. In the log-normal distribution we observe a tendency of λ to approach 1 as Δ increases, however, $P(r)$ (not shown in Fig. 1) becomes 0 before reaching it, due to the smaller value of Δ_{max} ($\Delta_{max} \approx 65$) in this case. Note that the steplike dependence of λ on Δ is due to the presence of the "integer part" function in Eq. (30). In Fig. 1(b) we show the functions $\lambda(\Delta)$ for the three cases (exponential, log-normal, power law) presented in Fig. 1(a), now with the inclusion of amplitude noise with $a = 0.9$. We observe that the time series with $\{r_n\}$ originating from a power distribution is practically unaffected by the presence of noise, in contrast to the exponentially generated r_n. The time series generated by r_n distributed according to the log-normal distribution is affected less than the exponential case. A remarkable difference is that, in the presence of noise, the distribution $P(r)$ for r_n containing a log-normal component is nonvanishing for a wider range of Δ values, i.e., noise leads to an increase in Δ_{max}. This is clearly shown in Fig. 1(d), where

we plot the distributions $P(r)$ for the three considered cases in the presence of amplitude noise with $a = 0.9$. Finally, in Fig. 1(c) we show the behavior of the function $R(\Delta)$ for the time series containing a power-law component in the noiseless (black line) as well as in the noisy (amplitude noise with $a = 0.9$; upper, red line) case; we observe the saturation of $R(\Delta)$ for $\Delta \gg 8$. Setting the asymptotic value of R in Eq. (31) we solve for p, finding $R = 1.68$ for both the noiseless and the noisy case. Due to finite statistics a small value of q (here $q \approx 0.01$) is required for the description of the simulated data. Note that the required q value decreases with increasing statistics and simultaneous decreasing size of the bin Δr used in the calculation of $P(r)$.

To explore further the insensitivity of $\lambda(\Delta)$ to noise effects in the case of power-law-distributed $\{r_n\}$, we consider also the influence of strong additive noise with $a = 5$. In this case the $P(r)$ distributions are strongly disordered as one can see in Fig. 2(a). No clear evidence of power-law behavior is observed in the distribution of r_n values containing a power-law component (red circles). Furthermore, the noise-affected distribution with a log-normal component vanishes quite rapidly at $r = \Delta_{max} \approx 100$. In Fig. 2(b) we observe
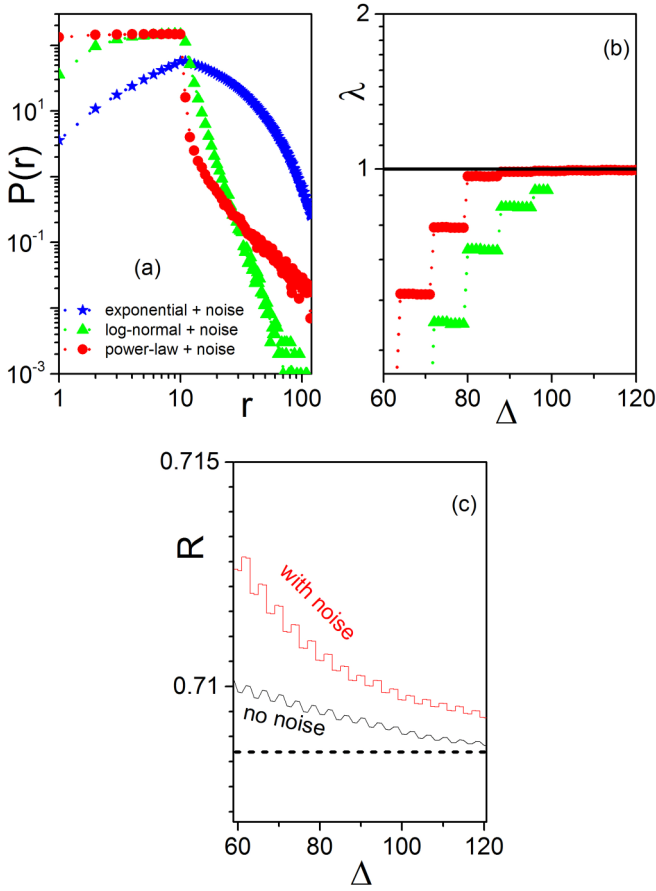
FIG. 2. Synthetic data with additive noise. (a) Distributions of the time-series values in the presence of additive noise with $a = 5$ for exponentially (blue stars), log-normally (green triangles), and power-law (red circles) distributed r_n. (b) Corresponding $\lambda(\Delta)$ functions for the log-normal (green triangles) and the power-law (red circles) cases. Note that the exponential does not fit at all in the presented window of λ. (c) The function $R(\Delta)$ for the power-law case comparing the noiseless (black line) with the noisy (upper, red line) case.
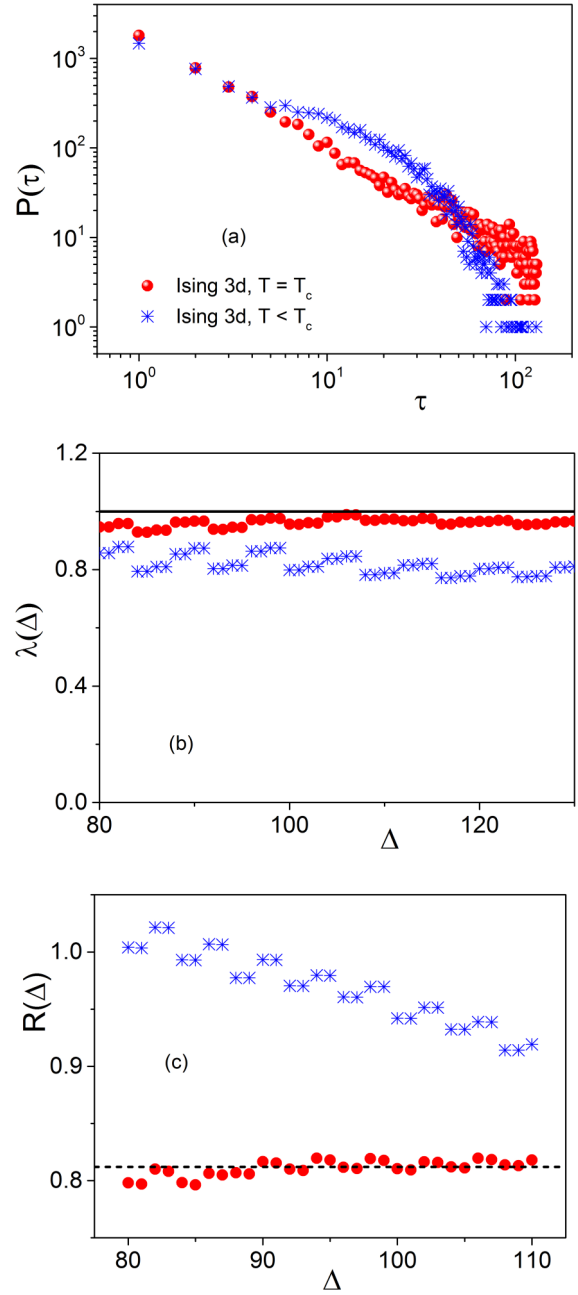

FIG. 3. Three-dimensional Ising simulated data. (a) Waiting-time distribution $P(\tau)$ for the 3D Ising model at $T = 4.545$ (red circles; pseudocritical) and $T = 4.45$ (blue stars). (b) The functions $\lambda(\Delta)$ for each case. (c) The function $R(\Delta)$ for both temperatures.

that, despite the damaged profile, the function $\lambda(\Delta)$, in the power-law case (red circles), still converges to 1 for $\Delta > 80$. In the same plot (Fig. 2(b)), it is shown, similarly to Fig. 1(a), that for the time series with a log-normal component (green triangles), the function $\lambda(\Delta)$ shows a tendency to approach the line $\lambda(\Delta) = 1$ but remains at a distance from it, since the corresponding distribution $P(r)$ becomes 0 before and the green points (triangles) stop when $\Delta = \Delta_{max} \approx 100$. In fact the decay of $P(r)$ is strongly influenced by the noise amplitude. Upon increasing a the maximally allowed value of Δ, i.e., the maximum value of r for which $P(r) \neq 0$ (in fact Δ_{max}), decreases significantly. Furthermore, Fig. 2(c) displays the remarkable stability of the function $R(\Delta)$ in the power-law case. We have considered also cases with even stronger additive noise and the observed robustness is sustained. However, with increasing a the range of allowed Δ values shrinks and the distributions $P(r)$ vanish rapidly, preventing the applicability of the proposed wavelet-based algorithm for $a > 10$.

Continuing with the applications of our approach we present one more characteristic example allowing the detection of power-law behavior in distributions obtained from simulated time series. It is obtained from the magnetization time series in the 3D Ising model simulation with the Metropolis algorithm. As shown in [19], the waiting times τ (measured in sweeps) in a narrow region around zero magnetization are power-law distributed with an exponent $p = 1 + \frac{1}{\delta}$, when $T = T_c$. For the 3D Ising model $\delta \approx 5$ (isothermal critical exponent), while T_c is the corresponding (pseudo)critical temperature for the ferromagnetic transition depending on the
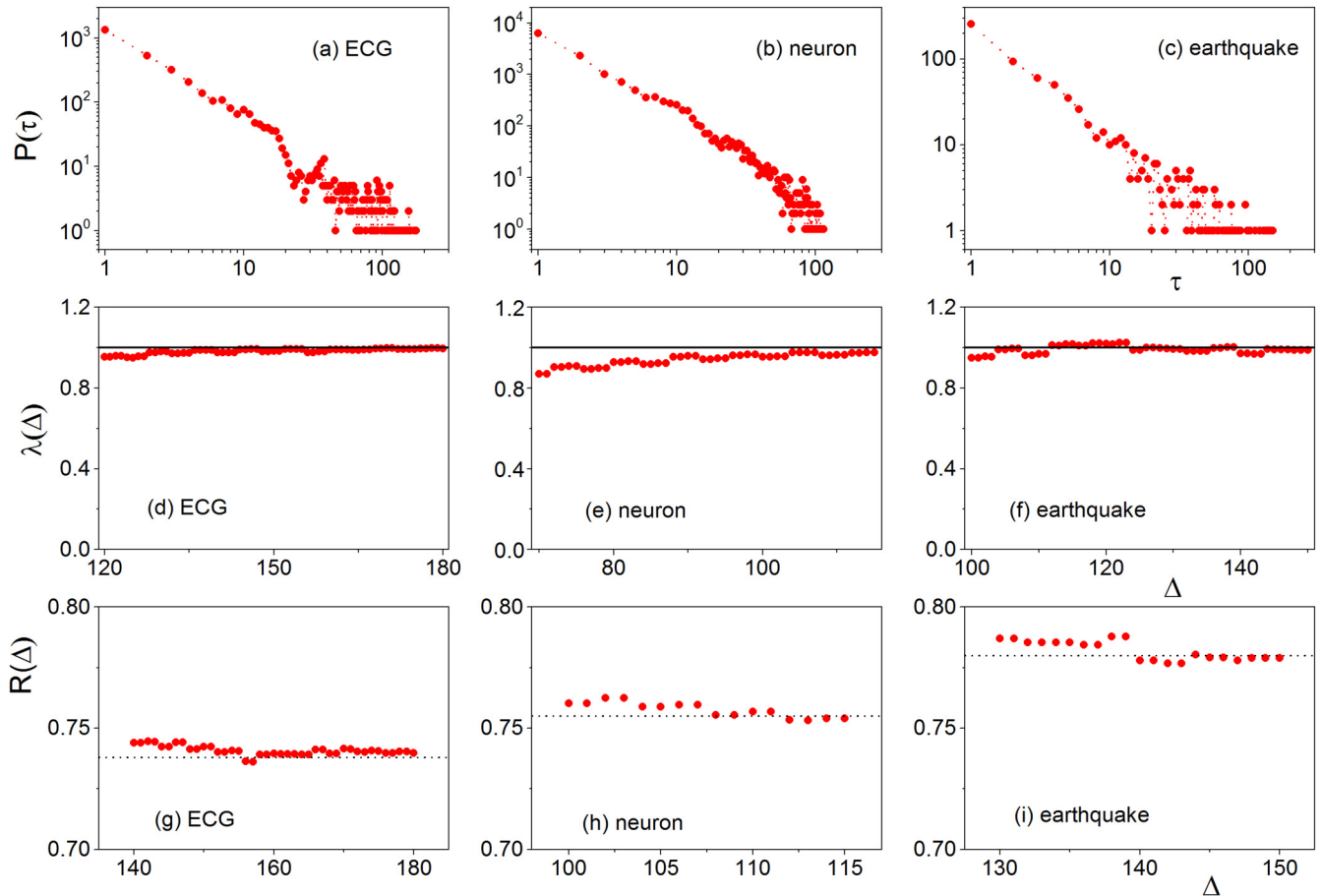
FIG. 4. Various experimental data. Waiting-time distribution $P(\tau)$ for (a) human ECG time series of healthy individuals (red circles), (b) membrane potential fluctuations of pyramidal neurons in the CA1 region of the rat hippocampus, and (c) preseismic electromagnetic emission in the MHz channel. (d)–(f) Corresponding functions $\lambda(\Delta)$. The black line at $\lambda = 1$ is a guide for the eye. (g)–(i) The function $R(\Delta)$ in the convergence region. A dotted line is used in each case to guide the eye.

lattice size. For $T < T_c$ the waiting-time distribution $P(\tau)$ attains an exponential tail. In Fig. 3(a) we plot $P(\tau)$ for $T \approx T_c$ (red circles) and $T < T_c$ (blue stars) using a simulated magnetization time series in a cubic lattice with $L = 20$. We observe a clear difference in the two distributions. This difference is clearly reflected also in the behavior of the corresponding functions $\lambda(\Delta)$ shown in Fig. 3(b). For $T = 4.545 \approx T_c$ the power-law behavior is imprinted in the property $\lambda \approx 1$ for a wide range of Δ values, while a deviation from criticality leads to the removal of the value 1 for $T = 4.45 < T_c$. In Fig. 3(c) we also show the function $R(\Delta)$ for the two cases. Clearly, for $T = 4.545$ there is no convergence. Using $R(\Delta)$ for $T \approx T_c$ in Eq. (31) we find the exponent $p = 1.18$, which is very close to $1 + \frac{1}{\delta}$ for the 3D Ising universality class ($\delta \approx 5$).

Before closing this section we present some examples demonstrating the application of the wavelet-based power-law detection (WBPLD) method to experimentally measured time series. In all examples the waiting-time distributions $P(\tau)$ around the most frequent value of the corresponding time series are calculated. In Figs. 4(a)–4(c) we plot these distributions. In Fig. 4(a) we show the distribution obtained from ECG time series for humans characterized as healthy [23]. In Fig. 4(b) is displayed the waiting-time distribution around the most frequent value of the membrane potential fluctuations

of pyramidal neurons in the CA1 region of a rat hippocampus [24]. Finally, Fig. 4(c) shows the waiting-time distribution around the most frequent value of the preseismic electromagnetic emission in the MHz channel [25]. In Figs. 4(d)–4(f) we show the corresponding $\lambda(\Delta)$ functions. The approach to 1 is evident, supporting the presence of power-law behavior in all three cases. The corresponding power-law exponents, calculated through R in Eq. (31), coincide with the values calculated in the literature with an accuracy of $< 1\%$. For completeness, in Figs. 4(g)–4(i) we show $R(\Delta)$ in the convergence region for each of the considered cases.

All the results of our analysis, including the estimation of the associated power-law exponents, are summarized in Table I.

V. CONCLUSIONS

We have developed a computational tool for the efficient detection of power-law behavior in distributions generated from experimentally recorded data. In contrast to the standard fitting procedures like least squares or maximum likelihood, which requires the adjustment of the parameters of the simulating function to optimally describe the observed distribution, in our method we first derive a number of properties

TABLE I. Δ_{max}, saturating R value, and power-law exponent p obtained from the waiting-time distributions in time series of simulated and experimentally recorded data. In the final column we also list the results obtained from a power-law fit neglecting the tail of the distribution.

Signal	Δ_{max}	R	p (fit)	p (WBPLD)
3D Ising	139	0.8082	1.18	1.18
Human ECG	180	0.7305	1.32	1.32
Rat neuron	115	0.7496	1.55	1.53
Earthquake	150	0.7753	1.31	1.31
Synthetic power law (with additive noise)	492	0.70784	1.81	1.68

characterizing the wavelet transform of the target distribution (power law in our case) independently from the value of the associated exponent and we subsequently search for the appearance of these properties in the experimental data. Using the Haar basis we can formulate the derived conditions analytically in terms of the analyzed signal. Having verified the presence of power-law behavior, the corresponding exponent is obtained solving an algebraic equation. The great advantage of this procedure is that due to the scaling properties of the wavelet basis, it is possible to observe power-law behavior which is valid only between two arbitrary scales which do not need to differ significantly. Finally, we have shown that the proposed scheme is capable of filtering windows of power-law behavior, at the same time allowing the safe estimation of the corresponding exponent, even in the presence of intensive noise. We have demonstrated the efficiency of our approach in a number of examples with increasing complexity. Thus, the proposed treatment introduces a novel strategy in the model description of experimentally observed data, providing an alternative to the standard fitting procedures. It would be interesting to perform our analysis employing different wavelet bases and checking their convergence properties for a wide set of experimental data, in an attempt to optimize the proposed scheme. This task will be considered in a future work.

APPENDIX: INFLUENCE OF NOISE

The influence of noise in the proposed wavelet analysis protocol for the detection of power laws is quantified by the small-scale fluctuations of $R(\Delta)$ in Eq. (31) in the saturation regime. In fact the function $R(\Delta)$ calculated from real data never becomes constant. The mean value $\langle R \rangle$ over an interval of Δ values saturates to a sufficient degree. The associated standard deviation $(\delta R)^2 = \langle R(\Delta)^2 \rangle - \langle R(\Delta) \rangle^2$ offers a suitable measure for quantification of the influence of noise on power-law data. This is clearly demonstrated in Fig. 5, where we plot the measure δR as a function of the noise amplitude for a power-law distribution contaminated with additive noise.

However, deformation of a power-law distribution is attributable not just to noise. As discussed in Sec. IV the noise induces exponential tails in a power-law distribution but the inverse is not always true. Exponential tails can also originate from other sources of deterministic origin like finite-size effects. This fact prevents the quantifibulletcation of noise ef-
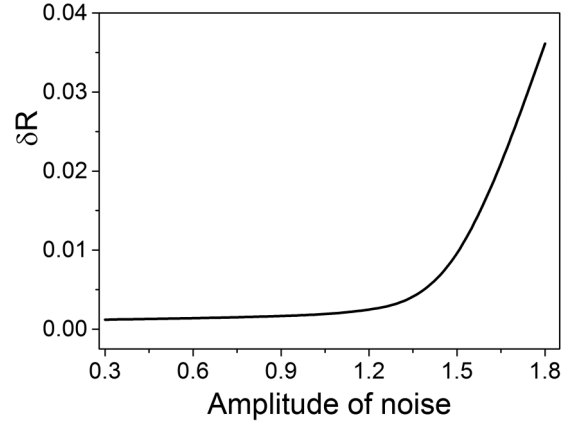

FIG. 5. Effect of noise. Dependence of the variance δR on the noise amplitude for the case of a power-law distribution contaminated with additive noise.

fects based on the magnitude of the characteristic exponent q in the function $h(i) = c i^{-p} \exp(-qi)$, leaving the quantity δR as the suitable one for the description of the influence of noise on a power-law distribution. Nevertheless, the use of $h(i)$ for the description of a power law deformed by an exponential tail turns out to be very efficient, despite the fact that there is no possibility of decoding the noise influence through the value of q. The latter is the reason why a theoretical link of the q value to the noise amplitude is lacking and we are left with empirical estimates.

A final remark in this Appendix concerns another aspect related to the influence of noise, namely, the exclusive use of $k = 0$ wavelet coefficients in the calculation of the quantities $\lambda(\Delta)$ and $r(\Delta)$ within our approach. An explanation is given in the paragraph below Eq. (31). Here we complete this line of argument, presenting in Fig. 6 a plot of the function $\lambda(\Delta)$ calculated using $j = 1$ and $k = 1$ in Eq. (11). The power-law
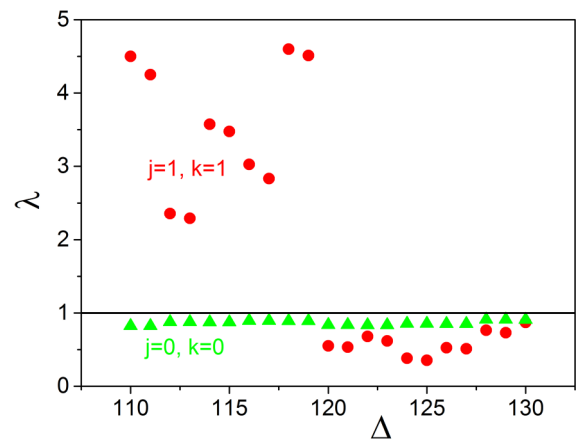

FIG. 6. Advantage of the $j = 0$, $k = 0$ description. The function $\lambda(\Delta)$ calculated using wavelet coefficients dictated by the choice $j = 1$, $k = 1$ in Eq. (11) (red circles). The calculation is based on a power-law distribution describing the waiting-time distribution of the magnetization time series in the 3D Ising model at the (pseudo)critical point. For comparison, $\lambda(\Delta)$ calculated using $j = 0$, $k = 0$ (green triangles) is also shown.

distribution, on which the calculation of $\lambda(\Delta)$ is based, is determined by the waiting times of the magnetization time series of the 3D Ising model at the critical temperature (see Fig. 3). We clearly observe the inability of the $j = 1$, $k = 1$ calculation (red circles) to reproduce the saturation at $\lambda = 1$ observed for the $j = 0$, $k = 0$ (green triangles) case.

[1] M. Schroeder, *Fractals, Chaos, Power Laws: Minutes from an Infinite Paradise* (Dover, Mineola, NY, 2009).

[2] P. Bak, *How Nature Works: The Science of Self-organized Criticality* (Springer, Berlin, 2013).

[3] B. Mandelbrot, *The Fractal Geometry of Nature* (Henry Holt and Company, New York, 1983).

[4] A. Clauset, C. R. Shalizi, and M. E. J. Newman, Power-law distributions in empirical data, SIAM Rev. **51**, 661 (2009).

[5] M. Farge, J. C. R. Hunt, and J. C. Vassilicos, *Wavelets, Fractals, and Fourier Transforms* (Clarendon Press, Oxford, UK, 1993).

[6] E. Foufoula-Georgiou and P. Kumar (eds.), *Wavelets in Geophysics* (Academic Press, New York, 1994).

[7] P. Abry, P. Goncalves, and J. L. Véhel, *Scaling, Fractals and Wavelets* (Wiley, New York, 2002).

[8] G. Rangarajan and M. Ding, *Processes with Long-Range Correlations: Theory and Applications* (Springer, Berlin, 2003).

[9] J. Pando and L.-Z. Fang, Discrete wavelet transform power spectrum estimator, Phys. Rev. E **57**, 3593 (1998).

[10] A. Arneodo, G. Grasseau, and M. Holschneider, Wavelet Transform of Multifractals, Phys. Rev. Lett. **61**, 2281 (1988).

[11] P. C. Ivanov, M. G. Rosenblum, C.-K. Peng, J. Mietus, S. Havlin, H. E. Stanley, and A. L. Goldberger, Scaling behaviour of heartbeat intervals obtained by wavelet-based time-series analysis, Nature **383**, 323 (1996).

[12] S. Janjarasjitt and K. A. Loparo, Examination of scale-invariant characteristics of epileptic electroencephalograms using wavelet-based analysis, Comput. Electr. Eng. **40**, 1776 (2014).

[13] D. L. Donoho and I. M. Johnstone, Ideal spatial adaptation by wavelet shrinkage, Biometrika **81**, 425 (1994).

[14] M. Lang, H. Guo, J. E. Odegard, C. S. Burrus, and R. O. Wells, Noise reduction using an undecimated discrete wavelet transform, IEEE Signal Process. Lett. **3**, 10 (1996).

[15] B. Walczak and D. L. Massart, Noise suppression and signal compression using the wavelet packet transform, Chem. Intel. Lab. Syst. **36**, 81 (1997).

[16] J. E. Fowler, The redundant discrete wavelet transform and additive noise, IEEE Signal Process. Lett. **12**, 629 (2005).

[17] M. Srivastava, C. L. Anderson, and J. H. Freed, A new wavelet denoising method for selecting decomposition levels and noise thresholds, IEEE Access **4**, 3862 (2016).

[18] U. Tanyeri and R. Demirci, Wavelet-based adaptive anisotropic diffusion filter, Adv. Electr. Comput. Eng. **18**, 99 (2018).

[19] Y. F. Contoyiannis, F. K. Diakonos, and A. Malakis, Intermittent Dynamics of Critical Fluctuations, Phys. Rev. Lett. **89**, 035701 (2002).

[20] G. Kaiser, *A Friendly Guide to Wavelets* (Birkhäuser, Boston 1994).

[21] C. K. Chui, *An Introduction to Wavelets* (Academic Press, New York, 1992).

[22] M. Abramowitz and I. Stegun, *Handbook of Mathematical Functions with Formulas, Graphs, and Mathematical Tables*, 9th ed. (Dover, Mineola, NY, 1972).

[23] Y. F. Contoyiannis, S. M. Potirakis, and K. Eftaxias, The Earth as a living planet : Human-type diseases in the earthquake preparation process, Nat. Hazards Earth Syst. Sci **13**, 125 (2013).

[24] E. K. Kosmidis, Y. F. Contoyiannis, C. Papatheodoropoulos, and F. K. Diakonos, Traits of criticality in membrane potential fluctuations of pyramidal neurons in the CA1 region of rat hippocampus, Eur. J. Neurosci. **48**, 2343 (2018).

[25] Y. F. Contoyiannis, P. G. Kapiris, and K. A. Eftaxias, Monitoring of a preseismic phase from its electromagnetic precursors, Phys. Rev. E **71**, 066123 (2005).